ARTICLE

Sub-Picosecond Photodynamics of Small Neutral Copper Oxide Clusters

Received 15th April 2024,
Accepted 00th January 20xx

DOI: 10.1039/x0xx00000x

Chase H. Rotteger,[1,2] Carter K. Jarman,[1,2] Madison M. Sobol,[1,2] Shaun F. Sutton,[1,2] and Scott G. Sayres[1,2,*]

The ultrafast dynamics of neutral copper oxide clusters (C_nO_x, n < 5) are reported using femtosecond pump probe spectroscopy in the gas phase. The transient spectra recorded for each cluster demonstrates they relax on a 100s of fs timescale followed by a long-lived (>50 ps) response. Density functional theory calculations are performed to determine the lowest energy structures and spin states. Topological descripters for the excited states are calculated (time-dependent density functional theory) to relate the measured excited state dynamics to changes in the cluster's electronic structure with increasing oxidation. Strong field ionization is demonstrated here to be a soft form of ionization and able to record transient signals for clusters previously determined to be unstable to nanosecond multiphoton ionization. The relative cluster stability is further demonstrated by signal enhancement/depreciation that is recorded through the synergy from the two laser pulses. Once the oxygen atoms exceed the number of copper atoms, a weakly bound superoxide O_2 unit forms, exhibiting a higher spin state. All clusters that are not in the lowest spin configuration demonstrate fragmentation.

1. Introduction

Bulk copper oxides are p-type semiconductors with two dominant stoichiometries, where Cu adopts an oxidation state of either +I (Cu_2O) or +II (CuO). Both have found application in a wide range of industries, including use as pigments,[1] sensors,[2] catalysts,[3] and semiconductor materials[4] due to their abundance, low-cost, and nontoxicity. Furthermore, copper oxides are effective antimicrobial agents,[5] where their high photocatalytic activity degrades organic pollutants[6,7] and prevents the accumulation of microorganisms for use in medicinal textiles and coatings. Both exhibit sufficient solar absorption and large charge-carrier separation for applications in photovoltaics,[8] optoelectronics, and light-emitting diodes.[9,10]

The properties of copper oxides are strongly dependent on stoichiometry, and related electron configurations. The band structure of Cu_2O is experimentally well established, having a dipole forbidden direct bandgap of 2.17 eV between the Cu-4s orbitals of the conduction band and the fully occupied Cu-3d orbitals of the valence band. In contrast, CuO has an indirect bandgap of 1.2 eV between open shells. The open shell nature of CuO enables good spin conductivity, but the filled 3d orbital of Cu_2O makes it a spin insulator.[11] Mixing the CuO and Cu_2O stoichiometries, or increasing defect and vacancy sites, enables its magnetic moment to be systematically tuned for spintronic applications.[12] The photodynamics measured in bulk copper oxides also show significant differences. Lifetimes of ~100s fs are attributed charge-carrier scattering in the valence band of nanostructured CuO followed by few-ps carrier-phonon relaxation and finally exciton recombination on 10s-100s of ps timescale.[13,14] In contrast, Cu_2O has extraordinarily long-lived (ns to µs) excited states (excitons) that are attributed to a parity forbidden orbital angular momentum coupling ($\Delta\ell$ = 2).[15] However, how these photodynamics properties translate to the sub-nanometer scale has not yet been explored.

There is great interest in adjusting the morphology of nanoscale copper oxides to select desirable electrochemical and catalytic traits. O_2 dissociation rates on Cu_n clusters increase as they grow in size, attributed to an energy of ~1.7 eV on the molecular scale and decreasing to < 0.4 eV on the nanometer scale.[16,17] Sub-nanometer clusters provide a pathway to efficiently reduce the cost of catalytic reactions by replacing precious metals, such as Ag, Pd, and Pt, in catalysts because of comparable catalytic efficiency and selectivity.[18] Copper cluster catalysts have been extensively studied for methanol synthesis from syngas (CO, CO_2, and H_2).[19] Significant attention has been garnered for the heterogeneous catalysis of supported, size-selected, and partially oxidized copper clusters.[16–22] In particular, substantial effort has been put into understanding the catalytic cycle of Cu_4.[19,21,23] However, characterization of the deposited clusters is challenging, and the working catalytic mechanism is still debated. The active catalysts may contain a range of isomers and important oxidation states. Transient oxidation states may be mechanistically relevant but missed by ensemble-averaged detection schemes. There is general agreement that the formation of high oxidation states of CuO

[a] School of Molecular Sciences, Arizona State University, Tempe, AZ 85287
[b] Biodesign Center for Applied Structural Discovery, Arizona State University, Tempe, AZ 85287
[c] *E-mail: Scott.Sayres@asu.edu
[d] Electronic Supplementary Information (ESI) available: The relative energy of several isomers for each cluster are presented in Figures S1-S4.

deactivates the catalysts surface, and that lower oxidation states are the driving species.

Gas phase studies provide access to a wider range of cluster stoichiometries, that often can be studied atom by atom, and therefore have potential to reveal how changes in oxidation affect the structure/function relationship. Although some clusters mimic defect sites, others exhibit entirely new properties. The properties of small copper oxide clusters are well explored. Subnanometer copper oxides catalyze many reactions where its efficacy and selectivity, sensitively depend on oxidation state.[24] Photoelectron spectroscopy has been applied to understand the electronic structure of Cu_1O_x,[25] Cu_2O_x,[26] and Cu_3O_x.[27] Collisional induced dissociation spectroscopy,[28] thermal desorption spectroscopy,[29] and ion mobility mass spectrometry[30] all show the instability of clusters containing more O than Cu atoms (above the $(CuO)_n$ stoichiometry) and suggests the heavily oxidized clusters contain weakly bound O_2 units. Density functional theory (DFT) calculations have explored the structures and properties of small copper oxide clusters.[30–37]

Despite the growing importance of copper oxide clusters, limited data is available regarding their excited state properties, which are of fundamental interest for photocatalytic applications. Here, we present experimental measurements of the charge-carrier photodynamics in small neutral copper oxide clusters (Cu_nO_x, $n < 5$) and employ DFT calculations to determine lowest energy structures between isomers and the relationship of excited state lifetimes and the charge carrier topology. We focus on small clusters, which exhibit a wide range of stoichiometries, from bare metal through the fully oxidized clusters of $(CuO)_n$. Our results demonstrate the experimentally measured lifetimes correlate with changes in the calculated excited state charge carrier properties with oxidation. We also present the stability of clusters with varying oxygen content, structure, and spin state. The transient dynamics of the larger clusters will be the subject of a subsequent manuscript.

2. Experimental Methods

Neutral copper oxide clusters are produced by laser ablation and the transient dynamics are measured using a home-built Wiley-McLaren[38] type time-of-flight mass spectrometer (TOF-MS) coupled to a fs laser. Our experimental apparatus has been described in detail in previous work.[39] Briefly, copper clusters are produced by ablating a 5 mm copper rod with the second harmonic of a Nd:YAG (532 nm) pulsed laser. The plasma plume is confined to a 1 x 60 mm collision cell to aid in copper oxide cluster formation and is directed with a 120-psi pulsed expansion of He gas seeded with 5% O_2. A molecular beam of only neutral clusters is formed as the clusters traverse a 2 mm diameter skimmer at a static voltage of -500V, which deflects all ionic species. Neutral clusters are ionized by a sequence of fs laser pulses for detection and separation through mass spectrometry. Cations produced from fs absorption are accelerated through a 105 cm field-free region by a ~4 kV electric field applied to the TOF extraction region. An Einzel lens focuses the clusters onto a microchannel plate (MCP) detector as they separate by their mass to charge ratios. A background pressure of ~7.5 x 10^{-7} Torr is maintained during operation by three turbomolecular pumps.

A fs pump pulse excites the neutral cluster to an intermediate excited state, containing an electron and hole pair (e^-—h^+ or exciton). This excitation initiates an ultrafast non-radiative relaxation mechanism where recombination ultimately transitions the electronic energy into vibrations or heat. This process is monitored using a probe pulse that ionizes the neutral cluster at a well-defined time delay enabling detection by mass spectrometry. Transient spectra are recorded by sending the 800 nm (1.55 eV) pulse through an optical delay stage, moving in 20 fs increments between ± 2.5 ps, and in 1 ps increments to ± 50 ps, with respect to the 400 nm (3.1 eV) pulse. The beams are recombined using a dichroic mirror and focused with a 50 cm focal lens to peak laser intensities of 1.4 x 10^{14} (400 nm) and 3.7 x 10^{14} W/cm^2 (800 nm). An average of 1000 mass spectra are recorded at each timestep. The ion intensity signal for each cluster is proportional to the excited state population remaining at each timestep. The laser intensities are minimized to limit ionization from either individual laser pulse and optimize transient signal obtained from the combined beams. Despite the laser intensities being much lower than we previously employed for the study of other metal oxide systems,[39–42] we record cluster distributions from either individual laser beams (Fig. 1).

Transient signals are analyzed using a combination of exponential decay and plateau functions, both convoluted with a Gaussian function accounting for the instrumental response function (measured as 35 fs through the cross correlation of Ar). The fitting parameters and extracted lifetimes (τ) are presented in Table 1. The contributions from both Cu isotopes (^{63}Cu and ^{65}Cu) are averaged prior to fitting. The plateau function is applied to account for ion signals which remain unchanged through the limits of the experimental delays (> 50 ps).

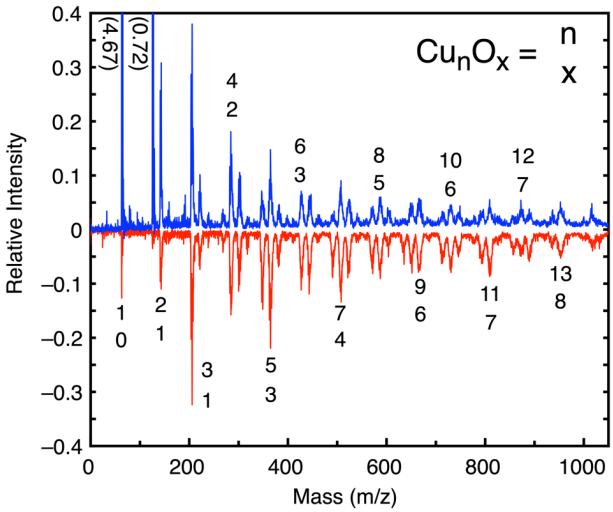

Fig. 1. Cu oxide cluster distribution for the individual 400 nm beam (blue) and 800 nm beam (inverted, red). The numbers in parenthesis are the relative intensities of the cropped Cu and Cu_2.

3. Computational Details

Geometry optimizations and time-dependent (TD)-DFT calculations for neutral copper oxide clusters are performed within the Gaussian16 software suite[43] using the CAM-B3LYP[44] and the 6-311G++(3d2f, 3p2d) basis set. This basis set is selected for its efficacy in describing the charge carrier distributions in our previous metal oxide studies[40] as it balances the Hartree-Fock exchange in the short and long range, enabling an accurate treatment of charge transfer associated with excited states. The excited state properties are beneficial for describing the initial charge transfer properties of the cluster upon photoabsorption of the pump pulse. Subsequent relaxation involves non-adiabatic coupling between the high-density of states, which is beyond the scope of this manuscript. Here, similar dynamics are recorded for both wavelengths serving as the pump beam and suggests that a rapid relaxation through the high density of states occurs. Thus, low-lying excited states are rapidly populated within the few 100s of fs presented. For simplicity, we limit our discussion to the excited state corresponding to the optical gap (O_{gap}) of each cluster, determined as the lowest energy excited state containing an oscillator strength (presented in Table 2). This state is sufficient as a general indicator of the electronic transitions. The excited state is composed of several electronic transitions, making transition densities the most straightforward representation of the e^- and h^+ distributions (presented next to the cluster structures in Figs. 2-5).

Several topological properties of the charge density are calculated to interpret the role of the e^- and h^+ interactions. The X-coordinate of the centroid of the electron is calculated through Eq. 1:

$$X_e = \int x\, \rho_e(r) dr \tag{1}$$

where ρ_e is electron density and x is the X component of the positional vector. The total distance between the centroids of the electron and hole is calculated with Eq. 2:

$$d = \sqrt{(d_x)^2 + \left(d_y\right)^2 + (d_z)^2} \tag{2}$$

where $d_x = |X_e\text{-}X_h|$ is the distance between the e^- and h^+ and is combined with the y and z dimensions to obtain total distance.

To determine the distribution breadths of the charge carriers, their root-mean-standard deviations (RMSD) are calculated as:

$$\sigma = \sqrt{\int (r-R)^2 \rho(r) dr} \tag{3}$$

where r is the distance from the centroid (R).

The well-known Λ index[45] quantifies the spatial overlap of the electron and hole wavefunctions, and ranges between 0 and 1 to describe completely separate or overlapping wavefunctions, respectively. The Λ value is calculated according to Eq. 4.

$$\Lambda = \frac{\sum_{o,v} c_{ov}^2 O_{ov}}{\sum_{o,v} c_{ov}^2} \tag{4}$$

The excitation involves occupied and unoccupied electrons, and the overlap of their spatial distributions (φ_o and φ_v) is calculated by Eq. 5.

$$O_{ov} = \int |\varphi_o||\varphi_v| dr \tag{5}$$

Charge carrier overlap is also described by the S_r index, utilizing densities rather than wavefunctions as:

$$S_r = \int \sqrt{\rho^{hole}(r)\rho^{ele}(r)} dr \tag{6}$$

Due to the relationship between wavefunction and density, the Λ and S_r values are the same for a pure transition, which is never the case for the copper oxide clusters.

In our previous studies of other metal oxide clusters, the delocalization of the e^- and h^+, the average of σ_e and σ_h, correlated with the measured lifetimes.[40] The h^+/e^- delocalization index (HDI/EDI) is similar to σ_e and σ_h but accounts for spatially separated localized densities across the cluster (Eqs. 7 and 8).

$$HDI = 100 \times \sqrt{\int [\rho^{hole}(r)]^2 dr} \tag{7}$$

$$EDI = 100 \times \sqrt{\int [\rho^{ele}(r)]^2 dr} \tag{8}$$

Smaller delocalization indexes describe larger charge carrier distributions. The HDI and EDI are found to be equally important and therefore are averaged to describe the total delocalization (TDI).

Through combination of the S_r and HDI/EDI equations, we present a new Γ index (Eq. 9), which provides insight into the spatial overlap and delocalization of the charge carriers.

$$\Gamma = 100 \times \sqrt{\int \rho^{hole}(r)\rho^{ele}(r)\, dr} \tag{9}$$

The charge carrier topological properties for the O_{gap} excited states for each cluster are presented in Table 2.

4. Results and Discussion

4.1 Neutral Cluster Distribution

Although it is not possible to definitively resolve the neutral copper oxide cluster distribution, the cation distribution recorded through fs ionization provides a reasonable picture of the neutral cluster beam and also highlights the stable clusters (Fig. 1). Relatively unstable clusters are recorded with low signal intensity in comparison to the more stable clusters in the mass spectrum. In our cluster distribution, $(Cu_2O)_n$ is most prevalent over the whole distribution, with additional mass peaks containing an extra Cu or O atom (Fig. 1). The $(Cu_2O)_n$ is more intense than its neighbouring peaks for small clusters (Cu_nO_x, n < 8), and transitions to $(Cu_2O)_nO$ as the largest signals for larger clusters, in agreement with previous studies.[29,46] Highly oxidized clusters have been shown to easily dissociate through collision,[28] heating,[29] and photoionization.[46] We record clusters in high oxidation states with SFI through either wavelength, including Cu_3O_2, Cu_4O_3, Cu_4O_4, Cu_5O_4, and Cu_6O_5, which are distinctly absent under ns-MPI conditions and limited to observation through single 118 nm photon (10.5 eV)

ionization.[46] Cluster signals arise here through strong-field ionization (SFI), demonstrating that the SFI is a softer form of ionization than multiphoton ns excitation.

It should be noted that clusters are not mass selected prior to ionization, so the measured ion signals may be influenced by fragmentation. Cu, Cu_2, and Cu_3 are nearly absent from the 800 nm distribution but are strong signals (~30x larger) from the isolated 400 nm laser beam (Fig. 1). Their absence from the 800 nm cluster distribution implies they are products of fragmentation from larger clusters by the 400 nm beam. Larger clusters are also more prominent in the 800 nm distribution, demonstrating it as softer ionization than the 400 nm, in agreement with relative Keldysh parameters. The Keldysh parameter, $\gamma = \sqrt{(IP/2U_P)}$, suggests tunneling ionization dominates for $\gamma << 1$.[47] Although this value is unique for each cluster according to its IP, we approximate it using a common value. Assuming an IP = 8, the 400 nm beam reaches a $\gamma = 1.4$, whereas the 800 nm beam reaches a $\gamma = 0.4$. Thus, the 800 nm signal is dominated by tunneling ionization whereas the 400 nm beam lies in the regime where tunneling competes with multiphoton absorption. Several clusters achieve different signal intensities depending on the laser pump sequence. This mismatch in signal intensity between long negative and positive time delays supports that SFI (using IR light) is less dissociative, than UV excitation (more MPI).

4.2 Lowest Energy Structures

A wide array of isomers and spin configurations are possible in the cluster beam resulting from the laser ablation process and are considered. Terminal O atoms are not predicted in the structures of larger clusters, however, terminal Cu atoms are a common feature. There is a strong propensity for Cu atoms to participate as bridging atoms between O atoms. Our calculations are consistent with reported geometries[30–33] and the lowest energy structures are reported next to their transient spectra in Figs. 2-5. In general, the Cu-O interaction is stronger than the Cu-Cu interaction and poor d-d mixing occurs. Although IPs have not been reported for the majority of the clusters, they provide insight to the relative intensity of the clusters. The cluster vertical IPs are calculated as the difference in energy between the cation and ground state at the same geometry. Both $\Delta s = \pm 1/2$ configurations are considered for the cation state. We calculate a vIP for CuO at 8.98 eV, in agreement with the experimental measurement (9.41 eV).[48] The bond length remains similar between neutral and cation structures, leading to large Franck-Condon overlap. Our calculations (Table 2) range between 6 and 8 eV for clusters containing more than one Cu atom. Ignoring the naked Cu_n series, the vIPs increase gradually with oxidation. Generally, the $(CuO)_n$ series have calculated IPs > 8.5 eV.[34] The IPs of Cu_3O_x increase almost linearly from x = 1 to 4 from (6 to 10 eV).[31] The HOMO-LUMO gap also increases from 1.6 eV to 2 eV upon a second O atom.[31] Clusters with high oxidation states have ferromagnetic coupling leading to high spin values. Oxygen rich clusters, defined here as having equal number of O and Cu atoms, are magnetic with ferromagnetic ordering, while oxygen poor clusters exhibit low spin configurations.[49] This is in contrast to bulk CuO, which has antiferromagnetic coupling.

4.3 Enhancement Factor

The stability of individual clusters is highlighted through measurement of the ion signal enhancement factors, E, which are defined here as the synergistic cluster signal intensity normalized to the summed signal of the individual 400 and 800 nm laser beams (Table 1). An $E > 1$ indicates either the formation of a long-lived excited state or the signal is also produced from the dissociation from a larger cluster. An $E < 1$ suggests fragmentation into smaller or less oxidized clusters, or the excited state moves into poor Franck-Condon overlap with the cation, thereby reducing the ionization efficiency. The relative E_{800} or E_{400} indicates the stability of clusters signals at long time delays, labelled according to the pump wavelength. Previous studies have shown that highly oxidized copper clusters are susceptible to fragmentation.[28] Our E measurements decrease with oxidation in agreement with reported relative stabilities.[28–30] Fragmentation is noted with increasing oxidation and spin state.

Table 1. The amplitudes (A) of the fitting coefficients for the excited state lifetimes (τ), and enhancement factors (E) for each cluster, each labelled according to the pump photon.

Cluster	A_{800}	τ_{800} (fs)	E_{800}	A_{400}	τ_{400} (fs)	E_{400}
Cu	1.6	164 ± 62	1.54	4.5	155 ± 58	4.28
CuO	2.4	264 ± 99	2.57	7.8	266 ± 31	2.70
CuO_2	1.1	223 ± 70	0.87	5.1	70 ± 10	0.96
CuO_3	0.0	< 35	0.74	0.0	< 35	0.74
Cu_2	0.0	< 35	1.84	1.3	261 ± 30	1.68
Cu_2O	0.7	181 ± 50	2.44	5.9	221 ± 9	1.95
Cu_2O_2	0.3	160 ± 42	0.91	2.7	92 ± 11	0.83
Cu_3	0.0	< 35	2.60	2.7	358 ± 44	2.23
Cu_3O	0.8	231 ± 103	2.95	6.8	244 ± 7	1.83
Cu_3O_2	0.5	207 ± 35	1.44	3.0	191 ± 12	1.08
Cu_3O_3	0.4	187 ± 44	0.90	1.8	153 ± 20	0.80
Cu_4O	0.7	335 ± 70	1.16	2.0	216 ± 18	1.02
Cu_4O_2	0.6	235 ± 72	1.67	3.5	188 ± 7	1.02
Cu_4O_3	0.6	173 ± 19	0.74	2.0	146 ± 7	0.56
Cu_4O_4	0.5	223 ± 63	0.69	1.4	85 ± 17	0.64

All clusters that are not in their lowest spin configuration exhibit an $E < 1$, suggesting that they are easily fragmented (release $^3O_2$). The reactivities/stabilities of the clusters are sensitive to the average oxidation number of the Cu atoms composing the cluster as the reaction cross sections increase with oxidation.[24] O_2 is suggested to be released from all clusters with large oxidation states, including Cu_3O_3, Cu_4O_3, and Cu_4O_4. These clusters also show $E < 1$ recorded for these clusters suggests that they also dissociate upon fs excitation. Such clusters have been suggested to contain an O_2 moiety that is easily released. In contrast, low oxidation state clusters such as Cu_3O and Cu_4O_2 are stable and exhibit large E. The measured E values are insensitive to small changes in laser intensity, and therefore demonstrate properties of the clusters themselves. The release of O_2 dominates reactions of $(CuO)_n$.[29] Clusters which may contain a weakly bound O_2 moiety fragment to a more stable cluster. The oxidation of supported Cu_n clusters

with O_2 is thermodynamically favorable until the $(CuO)_n$ stoichiometry is achieved.[22] The trends in each cluster series will be described separately.

4.4. The CuO_x Series Dynamics

The excited state lifetimes are measured for the clusters and labelled according to their pump wavelength, either when the 400 nm beam arrives first (τ_{400}, presented as positive time delay) or when the 800 nm beam arrives first (τ_{800}, presented as negative time delay). The transient signal for atomic Cu exhibits a strong Gaussian response and increases when pumped with 400 nm with a lifetime, τ_g, of 155 ± 58 fs, and then decays slightly (τ_{400} = 227 ± 31 fs) before reaching a plateau that lives beyond the timescale of the experiment (>> 50 ps). This long-lived Cu^+ signal aligns with previous measurements, reporting lifetimes on the 10s-100s of ns.[50] The growth after temporal overlap suggests that Cu^+ arises from the photodissociation of larger clusters. Both Cu and CuO decay within ~240 fs. The excited state lifetimes measured for the oxidized clusters pumped with 400 nm (τ_{400}) all decrease with oxidation (Fig. 2). CuO decays with similar lifetimes in positive and negative transients (τ_{400} = 266 ± 31 fs, τ_{800} = 264 ± 99 fs) with a large E = ~2.6. The Cu-O bond dissociation energy is 3 eV,[48,51] indicating that CuO may be unstable upon resonant 400 nm photoabsorption. However, the large E value suggests it is stable.

CuO_2 has an extremely fast relaxation timescale of τ_{400} = 70 ± 10 fs and a slower τ_{800} = 223 ± 70 fs. The lowest energy structure for CuO_2 has a Cu atom bound to O_2 where the single valance electron in Cu interacts with one O atom to form a superoxide configuration.[52] The O_2 unit may be the chromophore that absorbs near 400 nm leading to photodissociation and recovering the E = 1.[25] An energetically degenerate quartet linear form, O-Cu-O, is also found (Fig. S1).

CuO_3 is a weak signal in the mass spectra (Fig. 1) and exhibits only a Gaussian distribution in the temporal dynamics, matching the instrumental response function (35 fs). Our calculations suggest that CuO_3 contains a CuO bound to a superoxide type O_2 unit with a calculated vertical bond dissociation energy (BDE) of 1.84 eV ($^3O_2$). The low BDE coincides with the low ion intensity and Gaussian transient behavior of CuO_3. As noted earlier, such superoxides are relatively unstable, appear as small signals in our mass spectrum, and exhibit E < 1. Similarly, the loss of O_2 was recorded in photoexcitation of CuO_3^-.[25]

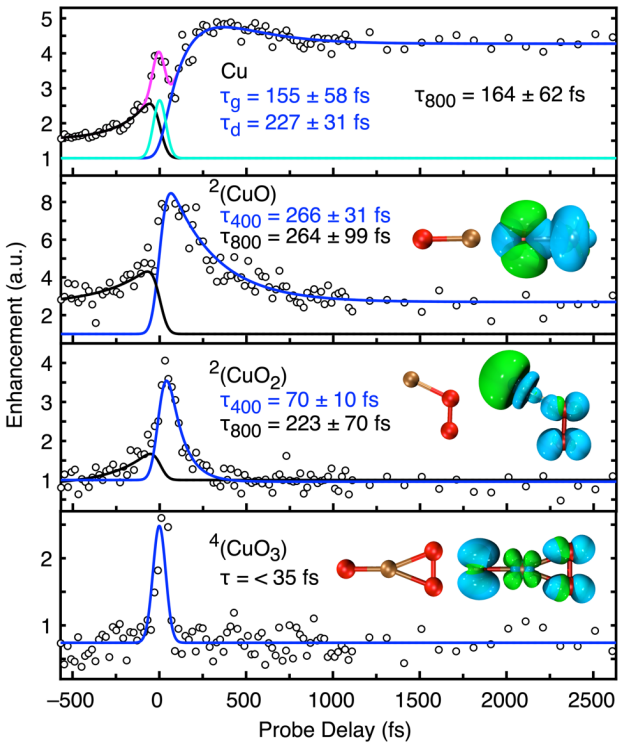

Fig. 2. Transient signals and lowest energy structures with corresponding spin for neutral CuO_x clusters (x = 0—3). TD-CAM-B3LYP transition densities, presented at an isodensity of 0.004 / Å^3. Electron density is shown in green, the hole is in blue, Cu atoms are orange, and oxygen are red. Note the y axis is unique to each cluster to indicate enhancement.

4.5. The Cu_2O_x Series Dynamics

The transient dynamics for the Cu_2O_x series exhibit similar behavior as the Cu_1O_x series (Fig. 3) in that the measured lifetimes decrease gradually upon the addition of O atoms. Cu_2 (IP = 7.9 eV) exhibits the slowest relaxation rate (τ_{400} = 261 ± 30 fs) before reaching a long-lived excited state with an E_{400} = 1.7. The τ_{800} is too small for measurement and reaches a larger E_{800} = 1.8. Photoexcitation of Cu_2 moves electron density from the bonding to antibonding orbitals. Cu_2O has a τ_{400} = 221 ± 9 fs and a large E_{400} = 2. The τ_{800} is similar at 181 ± 50 fs. The measured lifetimes for Cu_2O_2 of τ_{400} = 92 ± 11 fs, and τ_{800} = 160 ± 42 fs are both shorter and show an E < 1, suggesting fragmentation.

Our calculations imply that the Cu_2O_n series form nearly linear geometries. The lowest energy structure of Cu_2O is bent with a bond angle of 106.8° and Cu-O bond length of 1.78 Å, but the linear form is only 0.16 eV higher in energy (Fig. S2). Cu_2O_2 has two low energy isomers, both in spin triplet configurations. We find the linear form for Cu_2O_2 is the ground state, with a previously suggested rhombic structure being 0.19 eV higher in energy (Fig. S2). The Cu_2O_2 peroxide structure is not likely and is higher in energy (2.54 eV). Cu_2O_3 is not recorded, demonstrating a low stability. Two competitive isomers were calculated for Cu_2O_3, either containing a weakly bound $^3O_2$ or a linear form with a higher spin state (quintet).

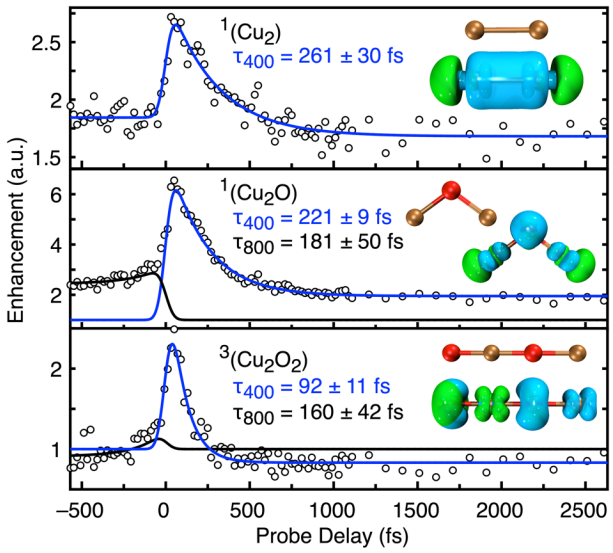

Fig. 3. Transient signals for neutral Cu_2O_x clusters (x = 0-2), similar to Fig. 2.

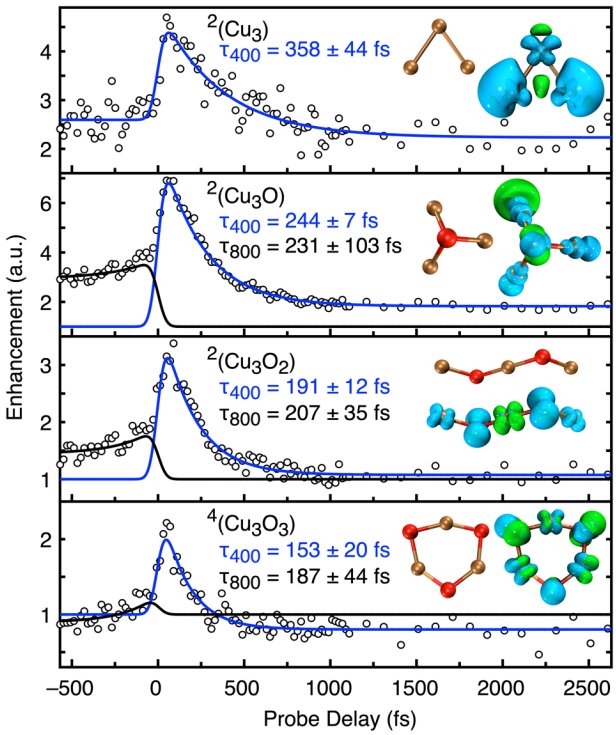

Fig. 4. Transient signals for neutral Cu_3O_x clusters (x = 0-3), similar to Fig. 2.

4.6. The Cu_3O_x Series Dynamics

The transient dynamics for the Cu_3O_x (Fig. 4) cluster series continue the trend recorded in the smaller cluster series. As oxidation increases within the series, the excited state lifetimes decrease. Less oxidized clusters have E > 1 and more oxidized clusters, such as Cu_3O_3 have E < 1, suggesting fragmentation. Cu_3 exhibits a τ_{400} = 358 ± 44 fs and a rapid τ_{800}, similar to Cu_2. Cu_3O exhibits a nearly identical τ_{400} of 244 ± 7 fs and τ_{800} = 231 ± 103 fs. Cu_3O is the most intense cluster in the distribution, has an extraordinarily low IP (6.18 eV), C_3 symmetry, and demonstrates the largest E at the temporal overlap of ~7. Cu_3O has been previously noted as particularly stable.[29]

The Cu_3O_2 has similar lifetimes in both directions with τ_{400} = 191 ± 12 fs and τ_{800} = 207 ± 35 fs, but an E_{800} > 1 is recorded, while the 400 nm pump signal recovers to baseline at long time delays (E_{400} = 1). Cu_3O_3 is also similar in both directions and recovers to baseline (E ~ 1), exhibiting τ_{400} = 153 ± 20 fs and τ_{800} = 187 ± 44 fs. This cluster appears to form a highly stable ground state ring structure, despite being in a higher spin state (quartet) and in agreement[27,32] with prior work. Alternative structures, containing an O_2 have also been proposed,[30] but not stable.

Cu_3O_4 is not observed and is thought to contain a weakly bound O_2 unit.[31] Our calculations for Cu_3O_4 match these results as we determine two degenerate lowest energy structures, one with a high spin state (sextet) and one with a weakly bound O_2 unit (Fig. S3). Our calculations for $Cu_3O_{3,4}$ match recent results.[27]

4.7. The Cu_4O_x Series Dynamics

Far less work has been applied to understand the gas-phase Cu_4O_x series.[29,30,36,49] Cu_4 is not produced in measurable quantities under these experimental conditions. It is also absent in high temperatures studies, despite small Cu_{1-3} clusters also being recorded.[29] The lowest energy structures for Cu_4O_x clusters are suggested to be planar, with intact Cu-Cu bonds.[36]

The Cu_4O_x clusters follow the same trend as all previous cluster series reported with a decrease in lifetimes with sequential oxidation (Fig. 5). However, in the Cu_4O_x series, the τ_{800} values are all evidently longer than τ_{400}. Cu_4O exhibits a τ_{400} = 216 ± 18 fs and a longer τ_{800} = 335 ± 70 fs, both with E = ~ 1. The lowest energy Cu_4O structure is 3D with each Cu atom participating in three Cu-Cu bonds and one Cu-O bond. A planar isomer lies 0.58 eV higher in energy.

Cu_4O_2 exhibits a τ_{400} = 188 ± 7 fs and the only large E in the series with a E_{800} = 1.7, indicating that increasing the number of Cu atoms in the clusters exhibit less enhancement when E > 1, aligning with fragmentation into smaller clusters created by the 400 nm beam (Fig. 1). Our calculations demonstrate that O atoms bridge the Cu atoms, enabling Cu_4O_2 to produce terminal Cu atoms. Cu_4O_2 has been previously noted to be the most stable oxide at high temperatures.[21] Cu_4O_2 is a planar structure that contains a rhombic Cu_2O_2 unit in its center and is terminated with Cu atoms. This structure highlights that the Cu_2O unit plays an important role in small cluster formation.

Cu_4O_3 and Cu_4O_4 both continue the decreasing lifetime trend with a τ_{400} = 146 ± 7 fs and τ_{400} = 85 ± 17 fs, respectively. Cu_4O_4 also has the greatest discrepancy between lifetimes with τ_{800} being ~2.5x larger than τ_{400}. Both clusters also measure the lowest enhancement out of all the clusters reported with E = ~0.6. Cu_4O_4 isomers have been previously shown to generally contain at least one atom that is easily abstracted[21] to form stable Cu_4O_3 clusters. All Cu_4O_4 isomers were calculated to have low O abstraction energies, matching our low E values.[21] In contrast, Cu_4O_3 isomers present highly variable O abstraction energies (with some > 2.3 eV).[21]

Table 2. The calculated parameters, including topological descriptors describing the excited state character, charge transfer character (Λ), S_r, distance between electron and hole density (d), average deviation of the electron and hole (σ_{eh}), Optical gap (O_g), vertical ionization potential (vIP).

Cluster	vIP (eV)	O_g (eV)	Λ	S_r	Γ	HDI (Å^{-3})	EDI (Å^{-3})	TDI (Å^{-3})	d (Å)	σ_h (Å^3)	σ_e (Å^3)	σ_{eh} (Å^3)
^{2}Cu	7.73	–	–	–	–	–	–	–	–	–	–	–
^{2}CuO	8.98	1.23	0.59	0.63	10.46	3.50	2.83	3.17	0.47	1.35	1.60	1.47
^{2}CuO$_2$	8.63	1.10	0.51	0.59	8.05	3.07	1.17	2.12	2.27	1.53	2.04	1.79
^{4}CuO$_3$	10.53	2.29	0.70	0.85	14.99	2.59	4.02	3.30	0.36	1.96	1.72	1.84
^{1}Cu$_2$	7.88	2.90	0.60	0.72	3.83	1.51	0.65	1.08	0.00	1.75	3.00	2.37
^{1}Cu$_2$O	7.75	1.77	0.46	0.49	6.76	3.50	0.98	2.24	0.92	1.41	2.96	2.18
^{3}Cu$_2$O$_2$	9.88	1.38	0.64	0.81	12.65	2.28	3.26	2.77	1.09	2.09	1.85	1.97
^{2}Cu$_3$	8.61	2.44	0.56	0.75	3.43	1.41	0.36	0.89	0.33	2.31	3.85	3.08
^{2}Cu$_3$O	6.18	1.23	0.75	0.83	4.58	1.19	0.77	0.98	0.77	2.39	2.97	2.68
^{2}Cu$_3$O$_2$	7.85	1.80	0.63	0.76	10.85	2.19	3.62	2.90	0.00	2.36	2.53	2.44
^{4}Cu$_3$O$_3$	9.48	0.43	0.65	0.79	11.21	2.39	2.30	2.34	0.31	2.02	2.10	2.06
^{1}Cu$_4$O	6.60	1.68	0.60	0.66	4.59	1.99	0.73	1.36	0.57	2.18	2.90	2.54
^{1}Cu$_4$O$_2$	6.79	1.71	0.48	0.57	4.38	3.11	0.65	1.88	0.00	2.25	4.45	3.35
^{3}Cu$_4$O$_3$	8.49	1.29	0.71	0.77	18.14	3.07	3.01	3.04	0.15	1.78	1.80	1.79
^{3}Cu$_4$O$_4$	8.48	1.39	0.72	0.80	19.44	3.38	2.98	3.19	0.03	1.76	1.83	1.80

Similar to the previous series, the highly oxidized clusters show fragmentation and are calculated to be high spin states with O_2 units. Our calculations suggest the lowest energy structures for Cu_4O_3 and Cu_4O_4 are both spin triplets. The lowest energy isomer of Cu_4O_3 has a Cu_2O_2 rhombic structure as a base connected to a Cu_2O unit. Cu_4O_3 has two other near degenerate triplet structures, however, neither contain an O_2 unit. This implicates that the high spin state for this cluster is the main driver for fragmentation compared to a weakly bound O_2 unit. Cu_4O_4 contains an O_2 peroxide unit with a high spin state and has a very low ion intensity in the mass spectrum compared to other clusters. The next lowest energy structure is square (C_{2v}) shaped and is 0.60 eV higher. The cube form[53] of Cu_4O_4 is calculated to be 1.4 eV higher in energy (Fig. S4). Cu_4O_5 is not observed through SFI, and Cu_4O_5 should be rewritten as $Cu_4O_3(O_2)$ because they all bear an O_2 dimer and are not stable with respect to O_2 desorption.[21] Our calculations result in a lowest energy quintet structure for Cu_4O_5 with a nearly degenerate triplet structure, both containing an O_2 unit.

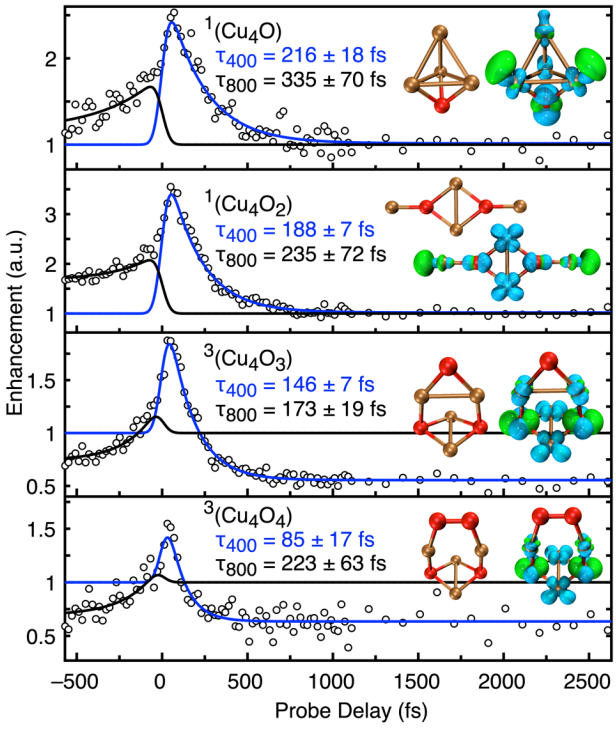

Fig. 5. Transient signals for neutral Cu_4O_x clusters (x = 1-4), similar to Fig. 2.

4.8. General Oxidation Effect

The transient dynamics measured for such small copper oxide clusters do not significantly change with cluster size, and all excited state lifetimes are recorded on the few hundred fs timescale. Despite this similarity, there is a consistent and clear decrease in lifetimes (τ) recorded with oxidation for each series. Furthermore, the enhancement factors demonstrate the increased propensity for fragmentation with oxidation.

Interpreting the trends recorded in transient signals across the cluster series is challenging due to fragmentation, along with a high density of excited states and competitive isomers. However, the topological descriptors of the charge carriers display general properties that account for the changing dynamics. The $d_{e\text{-}h}$ shows the charge carriers are both generally centered on the clusters. The σ_{eh} and TDI are similar concepts, and both show that the charge carriers generally become more localized with oxidation. The Λ and S_r indexes both quantify the e/h overlap, and the calculated values are all large (~0.6), indicating the bonds are more covalent than ionic in nature and therefore shows the charge transfer between Cu and O atoms is incomplete. Nevertheless, we make the typical assignment of a formal -2 oxidation state for the O atoms to assign the oxidation state of the complementary Cu atoms. We find that the lifetimes decrease almost linearly with increasing Cu oxidation state across the cluster series (Fig. 6). Furthermore, we show that in general the Γ index increases with oxidation. An increase in Γ correlates to increased localization and spatial overlap between the charge carriers, aligning with the expectation of decreasing measured lifetimes. Thus, the topological properties clearly demonstrate an increase in localization and overlap of the charge carrier densities with sequential oxidation.

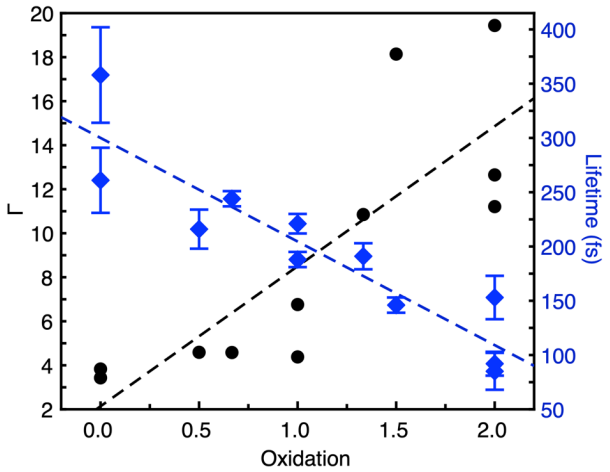

Fig. 6. The calculated Γ index (black) and experimentally measured lifetimes (blue) show a nearly linear change with the Cu oxidation state for each cluster. The points are fitted by the dashed lines with their respective color. Values from the CuO_x series are omitted due to their prominence from fragmentation.

Conclusions

The excited state lifetimes of small neutral copper oxide clusters are measured using femtosecond pump-probe spectroscopy to be sub-picosecond in duration and reach a long-lived state (>> 50 ps). The excited state lifetimes decrease with increasing oxidation. The signal enhancement value for each cluster shows the likelihood of fragmentation. Density functional theory calculations were performed to determine the lowest energy cluster structures. All clusters that are not in their lowest spin configuration exhibit an E < 1, suggesting that they are easily fragmented (release $^3O_2$). We show that clusters with high oxidation, increase the likelihood of a weakly bound O_2 in the structure and reside in a higher spin configuration. Time-dependent density functional calculations were performed to correlate the experimental trends to topological charge carrier properties. We show that the Γ index, which combines spatial overlap and delocalization of the charge carrier densities, generally aligns with the experimental lifetimes. The long-lived dynamics recorded for each cluster (indicated by E > 1) suggests that molecular scale copper oxides exhibit long lifetimes that may be employed for diverse applications.

Author Contributions

CHR and CKJ collected the experimental data. CHR and MMS performed the ab initio calculations, and SGS wrote the paper with contributions from all authors.

Conflicts of interest

There are no conflicts to declare.

Acknowledgements

We gratefully acknowledge support from ASU startup funds.

Notes and reference

1 M. Baneshi, S. Maruyama and A. Komiya, Comparison between aesthetic and thermal performances of copper oxide and titanium dioxide nano-particulate coatings, *Journal of Quantitative Spectroscopy and Radiative Transfer*, 2011, **112**, 1197–1204.
2 M. Balık, V. Bulut and I. Y. Erdogan, Optical, structural and phase transition properties of Cu_2O, CuO and Cu_2O/CuO: Their photoelectrochemical sensor applications, *Int. J. Hydrogen Energy*, 2019, **44**, 18744–18755.
3 A. Wang, J. Guan, L. Zhang, H. Wang, G. Ma, G. Fan, W. Tang, N. Han and Y. Chen, In Situ Synthesis of Monolithic Cu_2O–CuO/Cu Catalysts for Effective Ozone Decomposition, *J. Phys. Chem. C*, 2022, **126**, 317–325.
4 D. Gupta, S. R. Meher, N. Illyaskutty and Z. C. Alex, Facile synthesis of Cu_2O and CuO nanoparticles and study of their structural, optical and electronic properties, *J. Alloys Compd.*, 2018, **743**, 737–745.
5 S. Meghana, P. Kabra, S. Chakraborty and N. Padmavathy, Understanding the pathway of antibacterial activity of copper oxide nanoparticles, *RSC Adv.*, 2015, **5**, 12293–12299.
6 S. Wang, S. Gao, J. Tian, Q. Wang, T. Wang, X. Hao and F. Cui, A stable and easily prepared copper oxide catalyst for degradation of organic pollutants by peroxymonosulfate activation, *J. Hazard. Mater.*, 2020, **387**, 121995.
7 B. A. Koiki and O. A. Arotiba, Cu_2O as an emerging semiconductor in photocatalytic and photoelectrocatalytic treatment of water contaminated with organic substances: a review, *RSC Adv.*, 2020, **10**, 36514–36525.

8 A. Bhaumik, A. Haque, P. Karnati, M. F. N. Taufique, R. Patel and K. Ghosh, Copper oxide based nanostructures for improved solar cell efficiency, *Thin Solid Films*, 2014, **572**, 126–133.
9 İ. Y. Erdoğan and Ö. Güllü, Optical and structural properties of CuO nanofilm: Its diode application, *J. Alloys Compd.*, 2010, **492**, 378–383.
10 T. Zhou, Z. Zang, J. Wei, J. Zheng, J. Hao, F. Ling, X. Tang, L. Fang and M. Zhou, Efficient charge carrier separation and excellent visible light photoresponse in Cu_2O nanowires, *Nano Energy*, 2018, **50**, 118–125.
11 R. Sha, Q. Liu, M. Wang, M. Liu, Y. Peng, Z. Zhang, A. Zou, Y. Xu, X. Jiang and Z. Qiu, Spin transport in different oxide phases of copper, *Phys. Rev. B*, 2021, **103**, 024432.
12 A. Sumanth, V. Mishra, P. Pandey, M. S. R. Rao and T. Dixit, Investigations Into the Role of Native Defects on Photovoltaic and Spintronic Properties in Copper Oxide, *IEEE Trans. Nanotechnology*, 2022, **21**, 522–527.
13 B. Born, J. D. A. Krupa, S. Geoffroy-Gagnon, I. R. Hristovski, C. M. Collier and J. F. Holzman, Ultrafast Charge-Carrier Dynamics of Copper Oxide Nanocrystals, *ACS Photonics*, 2016, **3**, 2475–2481.
14 T. Dimopoulos, A. Peić, P. Müllner, M. Neuschitzer, R. Resel, S. Abermann, M. Postl, E. J. W. List, S. Yakunin, W. Heiss and H. Brückl, Photovoltaic properties of thin film heterojunctions with cupric oxide absorber, *J. Renew. Sustain. Energy*, 2013, **5**, 011205.
15 D. Fishman, C. Faugeras, M. Potemski, A. Revcolevschi and P. H. M. Van Loosdrecht, Magneto-optical readout of dark exciton distribution in cuprous oxide, *Phys. Rev. B*, 2009, **80**, 045208.
16 P. Concepción, M. Boronat, S. García-García, E. Fernández and A. Corma, Enhanced Stability of Cu Clusters of Low Atomicity against Oxidation. Effect on the Catalytic Redox Process, *ACS Catal.*, 2017, **7**, 3560–3568.
17 E. Fernández, M. Boronat and A. Corma, Trends in the Reactivity of Molecular O_2 with Copper Clusters: Influence of Size and Shape, *J. Phys. Chem. C*, 2015, **119**, 19832–19846.
18 A. Halder, M. Ha, H. Zhai, B. Yang, M. J. Pellin, S. Seifert, A. N. Alexandrova and S. Vajda, Oxidative Dehydrogenation of Cyclohexane by Cu *vs* Pd Clusters: Selectivity Control by Specific Cluster Dynamics, *ChemCatChem*, 2020, **12**, 1307–1315.
19 C. Liu, B. Yang, E. Tyo, S. Seifert, J. DeBartolo, B. Von Issendorff, P. Zapol, S. Vajda and L. A. Curtiss, Carbon Dioxide Conversion to Methanol over Size-Selected Cu_4 Clusters at Low Pressures, *J. Am. Chem. Soc.*, 2015, **137**, 8676–8679.
20 B. Zandkarimi, G. Sun, A. Halder, S. Seifert, S. Vajda, P. Sautet and A. N. Alexandrova, Interpreting the Operando XANES of Surface-Supported Subnanometer Clusters: When Fluxionality, Oxidation State, and Size Effect Fight, *J. Phys. Chem. C*, 2020, **124**, 10057–10066.
21 G. Sun, A. N. Alexandrova and P. Sautet, Structural Rearrangements of Subnanometer Cu Oxide Clusters Govern Catalytic Oxidation, *ACS Catal.*, 2020, **10**, 5309–5317.
22 S. K. Iyemperumal, T. G. Fenton, S. L. Gillingham, A. D. Carl, R. L. Grimm, G. Li and N. A. Deskins, The stability and oxidation of supported atomic-size Cu catalysts in reactive environments, *J. Chem. Phys.*, 2019, **151**, 054702.
23 S. Sharma and A. Ansari, Metal and metal oxide sub nano cluster; emerging aspirant for catalytic applications, *Results Chem.*, 2023, **5**, 100982.
24 S. Hirabayashi and M. Ichihashi, Gas-Phase Reactions of Copper Oxide Cluster Cations with Ammonia: Selective Catalytic Oxidation to Nitrogen and Water Molecules, *J. Phys. Chem. A*, 2018, **122**, 4801–4807.
25 H. Wu, S. R. Desai and L.-S. Wang, Chemical Bonding between Cu and Oxygen-Copper Oxides vs O_2 Complexes: A Study of CuO_x (x = 0-6) Species by Anion Photoelectron Spectroscopy, *J. Phys. Chem. A*, **101**, 2103–2111.
26 L.-S. Wang, H. Wu, S. R. Desai and L. Lou, Electronic structure of small copper oxide clusters: From Cu_2O to Cu_2O_4, *Phys. Rev. B*, 1996, **53**, 8028–8031.
27 X.-L. Xu, B. Yang, Z.-Y. Wei, G.-J. Cao, H.-G. Xu and W.-J. Zheng, Structural and bonding properties of $Cu_3O_3^-$ and $Cu_3O_4^-$ clusters: anion photoelectron spectroscopy and density functional calculations, *Phys. Chem. Chem. Phys.*, 2018, **20**, 20622–20628.
28 J. R. Gord, R. J. Bemish and B. S. Freiser, Collision-induced dissociation of positive and negative copper oxide cluster ions generated by direct laser desorption/ionization of copper oxide, *Int. J. Mass Spectrom. Ion Processes*, 1990, **102**, 115–132.
29 H. Wang, K. Miyajima, S. Kudoh and F. Mafuné, Effect of atomicity on the oxidation of cationic copper clusters studied using thermal desorption spectrometry, *Phys. Chem. Chem. Phys.*, 2019, **21**, 23129–23135.
30 M. Abdul Latif, J. W. J. Wu, R. Moriyama, M. Nakano, K. Ohshimo and F. Misaizu, Stable Compositions and Structures of Copper Oxide Cluster Cations $Cu_nO_m^+$ (n = 2–8) Studied by Ion Mobility Mass Spectrometry, *ACS Omega*, 2018, **3**, 18705–18713.
31 G. Bae, Structures and Electronic Properties of Cu_3O_N (N = 1–6) Clusters using *ab initio* Monte Carlo Simulations, *Bull. Korean Chem. Soc.*, 2016, **37**, 638–642.
32 G.-T. Bae, B. Dellinger and R. W. Hall, Density Functional Calculation of the Structure and Electronic Properties of Cu_nO_n (n = 1−8) Clusters, *J. Phys. Chem. A*, 2011, **115**, 2087–2095.
33 G.-T. Bae, Structure and electronic properties of copper oxide clusters and the effect of reacting with water investigated using Monte Carlo simulations and DFT calculations, *Comput. Theor. Chem.*, 2021, **1204**, 113377.
34 S. Das, S. Nigam, P. Sharma and C. Majumder, Evolution of the Atomic and Electronic Structures of CuO Clusters: A Comprehensive Study Using DFT Approach, *Phys. Chem. Chem. Phys.*, 2024, accepted.
35 C. Ramanathan, S. Subramanian and R. Valantina, Structural and Electronic Properties of CuO, CuO_2 and Cu_2O Nanoclusters - a DFT Approach, *Mater. Sci.*, 2015, **21**, 187–190.
36 N. Mammen, L. Spanu, E. C. Tyo, B. Yang, A. Halder, S. Seifert, M. J. Pellin, S. Vajda and S. Narasimhan, Reversing Size-Dependent Trends in the Oxidation of Copper Clusters through Support Effects, *Eur. J. Inorg. Chem.*, 2018, **2018**, 16–22.
37 B. Shi, S. Weissman, F. Bruneval, L. Kronik and S. Öğüt, Photoelectron spectra of copper oxide cluster anions from first principles methods, *J. Chem. Phys.*, 2018, **149**, 064306.
38 W. C. Wiley and I. H. McLaren, Time-of-Flight Mass Spectrometer with Improved Resolution, *Rev. Sci. Instrum.*, 1955, **26**, 1150–1157.
39 J. M. Garcia, R. E. Shaffer and S. G. Sayres, Ultrafast pump–probe spectroscopy of Neutral Fe_nO_m Clusters (n , m < 16), *Phys. Chem. Chem. Phys.*, 2020, **22**, 24624–24632.
40 J. M. Garcia, L. F. Heald, R. E. Shaffer and S. G. Sayres, Oscillation in Excited State Lifetimes with Size of Sub-nanometer Neutral $(TiO_2)_n$ Clusters Observed with Ultrafast Pump–Probe Spectroscopy, *J. Phys. Chem. Lett.*, 2021, **12**, 4098–4103.
41 J. M. Garcia and S. G. Sayres, Increased Excited State Metallicity in Neutral Cr_2O_n Clusters (n < 5) upon Sequential Oxidation, *J. Am. Chem. Soc.*, 2021, **143**, 15572–15575.
42 J. M. Garcia and S. G. Sayres, Orbital-dependent photodynamics of strongly correlated nickel oxide clusters, *Phys. Chem. Chem. Phys.*, 2022, **24**, 5590–5597.
43 M. J. Frisch, G. W. Trucks, H. B. Schlegel, G. E. Scuseria, M. A. Robb, J. R. Cheeseman, G. Scalmani, V. Barone, B. Mennucci, G. A. Petersson, H. Nakatsuji, M. Caricato, X. Li, H. P. Hratchian, A. F. Izmaylov, J. Bloino, G. Zheng, J. L. Sonnenberg, M. Hada, M. Ehara, K. Toyota, R. Fukuda, J. Hasegawa, M. Ishida, T. Nakajima, Y. Honda, O. Kitao, H. Nakai, T. Vreven, J. A. Montgomery Jr., J. E. Peralta, F. Ogliaro, M. Bearpark, J. J. Heyd, E. Brothers, K. N. Kudin, V. N. Staroverov, R. Kobayashi, J. Normand, K. Raghavachari, A. Rendell, J. C. Burant, S. S. Iyengar, J. Tomasi, M. Cossi, N. Rega, J. M. Millam, M. Klene, J. E. Knox, J. B. Cross, V. Bakken, C. Adamo, J. Jaramillo, R. Gomperts, R. E. Stratmann, O. Yazyev, A. J. Austin, R. Cammi, C. Pomelli, J. W. Ochterski, R. L. Martin, K. Morokuma, V. G. Zakrzewski, G. A. Voth, P. Salvador, J. J. Dannenberg, S. Dapprich, A. D. Daniels, O. Farkas, J. B. Foresman, J. V. Ortiz, J. Cioslowski and D. J. Fox, Gaussian16 (Revision A.03), Gaussian Inc. Wallingford CT.
44 T. Yanai, D. P. Tew and N. C. Handy, A new hybrid exchange–correlation functional using the Coulomb-attenuating method (CAM-B3LYP), *Chem. Phys. Lett.*, 2004, **393**, 51–57.
45 M. J. G. Peach, P. Benfield, T. Helgaker and D. J. Tozer, Excitation energies in density functional theory: An evaluation and a diagnostic test, *J. Chem. Phys.*, 2008, **128**, 044118.
46 Y. Matsuda, D. N. Shin and E. R. Bernstein, On the copper oxide neutral cluster distribution in the gas phase: Detection through 355 nm and 193 nm multiphoton and 118 nm single photon ionization, *J. Chem. Phys.*, 2004, **120**, 4165–4171.
47 L. V. Keldysh, Ionization in Field of a Strong Electromagnetic Wave, *Sov. Phys. JETP*, 1965, **20**, 1307–1314.
48 R. B. Metz, C. Nicolas, M. Ahmed and S. R. Leone, Direct determination of the ionization energies of FeO and CuO with VUV radiation, *J. Chem. Phys.*, 2005, **123**, 114313.

49 F. Yang, Q. Sun, L. L. Ma, Y. Jia, S. J. Luo, J. M. Liu, W. T. Geng, J. Y. Chen, S. Li and Y. Yu, Magnetic Properties of Cu_mO_n Clusters: A First Principles Study, *J. Phys. Chem. A*, 2010, **114**, 8417–8422.
50 K. Fu, M. Jogwich, M. Knebel and K. Wiesemann, Atomic transition probabilities and lifetimes for the CuI system, *At. Data Nucl. Data Tables*, 1995, **61**, 1–30.
51 I. S. Parry, A. C. Hermes, A. Kartouzian and S. R. Mackenzie, Imaging the photodissociation dynamics of neutral metal clusters: copper dimer, Cu_2, and copper oxide, CuO, *Phys. Chem. Chem. Phys.*, 2014, **16**, 458–466.
52 K. Pradhan, G. L. Gutsev, C. A. Weatherford and P. Jena, A systematic study of neutral and charged 3d-metal trioxides and tetraoxides, *J. Chem. Phys.*, 2011, **134**, 144305.
53 A. Halder, J. Kioseoglou, B. Yang, K. L. Kolipaka, S. Seifert, J. Ilavsky, M. Pellin, M. Sowwan, P. Grammatikopoulos and S. Vajda, Nanoassemblies of ultrasmall clusters with remarkable activity in carbon dioxide conversion into C1 fuels, *Nanoscale*, 2019, **11**, 4683–4687.

ARTICLE

Insert Table of Contents artwork here

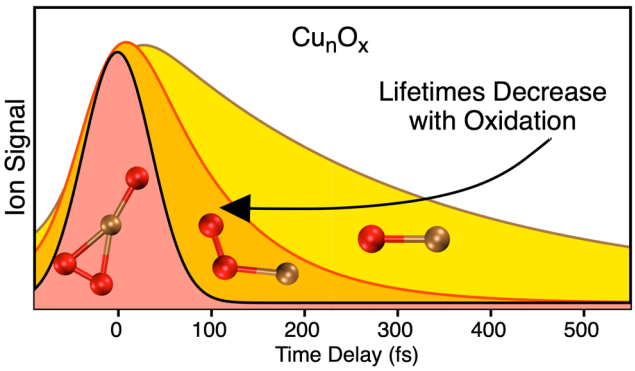

TOC label: The excited state lifetimes of small neutral copper oxide clusters decrease with oxidation on the sub-picosecond timescale.